PCCP

Accepted Manuscript

ROYAL SOCIETY OF CHEMISTRY

www.rsc.org/pccp

Journal Name

RSCPublishing

ARTICLE

Self-assembly and coverage dependent thermally induced conformational changes of Ni(II)-*meso*-tetrakis (4-tert-butylphenyl) benzoporphyrin on Cu(111)

Cite this: DOI: 10.1039/x0xx00000x

Received 00th January 2012,
Accepted 00th January 2012

DOI: 10.1039/x0xx00000x

www.rsc.org/

Liang Zhang[a,b], Michael Lepper[a,b], Michael Stark[a,b], Dominik Lungerich[b,c], Norbert Jux[b,c], Wolfgang Hieringer[b,d], Hans-Peter Steinrück[a,b], and Hubertus Marbach[*a,b]

A systematic scanning tunnelling microscopy investigation of the self-assembly and of thermally induced conformational changes of Ni(II)-*meso*-tetrakis (4-tert-butylphenyl) benzoporphyrin (Ni-TTBPBP) on Cu(111) is presented. At room temperature, Ni-TTBPBPs diffuse on the surface and self-assemble into ordered islands with well-defined registry to the substrate, with two different azimuthal orientations. The formation of the characteristic supramolecular structure is attributed to van der Waals interactions between the tert-butyl groups. Upon moderate heating, the intramolecular conformation changes irreversibly due to a dehydrogenative intramolecular aryl-aryl coupling reaction. This reaction is coverage dependent, with a lower rate at higher initial coverage; this behaviour is attributed to a stabilization of Ni-TTBPBP in the ordered islands at higher coverage.

Introduction

The self-assembly of molecular building blocks into highly-ordered nanoarchitectures on well-defined surfaces is an important approach towards the creation of novel materials with outstanding properties[1-7]. For such a bottom-up strategy, the investigation of the adsorption behaviour of large organic molecules on single-crystal metal surfaces has become a fast growing field in surface science[2, 5-8]. Firstly, one gains insight into the interaction between complex organic molecules and solid substrates, which is a key issue for the development of functional interfaces and plays an essential role in the engineering of nanoscale architectures on surfaces. Secondly, it opens up a new avenue to gain deeper insight into fundamental properties and thus the functionality of the utilized molecular building blocks. In this respect, scanning tunnelling microscopy (STM) is a powerful tool to investigate such systems in real space[7, 9-11].

One important group of such organic molecules are porphyrins, which have numerous technological applications due to their versatile functionalities and distinct chemical and physical properties[12, 13]. During the past few years, extensive attention has been paid to porphyrins self-assembled on metal surfaces in order to gain more information about their electronic properties, inherent conformational flexibility and reactivity[4, 14-27]. It has been demonstrated that the adsorption behaviour of porphyrins, such as intramolecular conformation and supramolecular arrangement, is strongly dependent on the actual substrate[5, 21, 28], the coverage of these molecules[22], the surface temperature[4, 23, 29] and the functional side groups of the porphyrin macrocycle[5, 24, 30, 31].

Generally, the adsorption behaviour is determined by the subtle balance between molecule-molecule and molecule-substrate interactions. For instance, individual 2H-tetraphenylporphrin (2H-TPP) molecules can be observed by STM on Cu(111) even at room temperature, due to the strong molecule-substrate interaction in between the iminic nitrogen atoms of the porphyrin and the Cu atoms of the substrate[21, 32]. In contrast, on Ag(111) supramolecular arrangements of 2H-TPP are formed, which is caused by the T-type intermolecular interactions between the peripheral phenyl substituents of neighbouring molecules[28, 33]. Alternatively, by appropriate functionalization of the tetrapyrrole ring of porphyrin, the molecule-molecule and molecule-substrate interactions can be effectively tailored. For example, porphyrins anchored with carboxyl groups form two-dimensional hydrogen-bonded networks, which are quite different from the close-packed arrangement without hydrogen bonds[25]. In addition, an

unprecedented type of linking is found between porphyrin molecules functionalized with methyl groups[24]. For a more general understanding, it is therefore of great importance to design novel porphyrin derivatives with different functional groups and to investigate their adsorption behaviour, in order to gain insight into the influence of these substituents on the self-assembly process, the electronic properties and the bonding mechanisms.

In this work, we present a detailed investigation of the self-assembly and temperature-dependent conformations of Ni(II)-*meso*-tetrakis (4-tert-butylphenyl) benzoporphyrin (Ni-TTBPBP) on Cu(111) by STM. Figure 1 shows the chemical structure of Ni-TTBPBP, in which four tert-butyl phenyl (tBP) groups and benzene rings are substituted to the meso- and β-positions of a central porphyrin macrocycle, respectively. Our experimental results demonstrate that upon deposition at room temperature, Ni-TTBPBP molecules self-assemble into large-area supramolecular domains with a square unit cell, due to van der Waals forces between the adjacent tBP groups of neighbouring molecules. Notably, upon moderate annealing the intramolecular conformation changes significantly, which can mainly be attributed to the intramolecular aryl-aryl coupling reaction of Ni-TTBPBP.

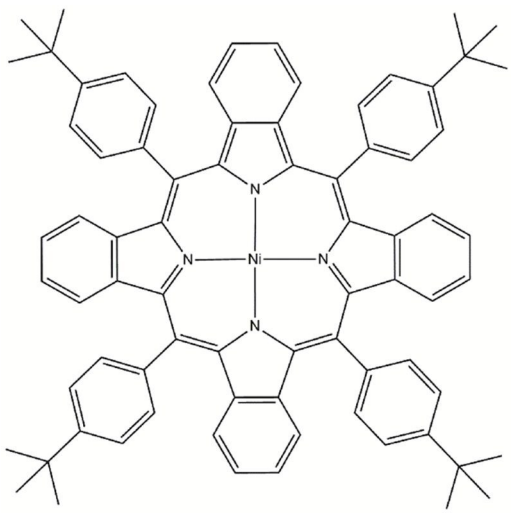

Figure 1. Chemical Structure of Ni-TTBPBP.

Experimental and Computational Details

The experiments and sample preparations were performed in a two-chamber ultrahigh vacuum (UHV) system with a base pressure of ~10^{-10} mbar. The microscope is an RHK UHV VT STM 300 with RHK SPM 200 electronics. The STM images were acquired at room temperature (RT) or at 200 K in constant current mode with a Pt/Ir tip. The given bias voltages refer to the sample. The STM images were processed with WSxM software and moderate filtering (Gaussian smooth, background subtraction) was applied for noise reduction[34]. The Cu(111) single crystal was prepared by repeated cycles of Ar^+ sputtering (500 eV) and annealing to 850 K. The Ni-TTBPBP molecules were deposited onto the Cu substrate at RT by thermal sublimation from a home-built Knudsen cell at 690 K. The <110> axes of the Cu(111) surface were determined by depositing 2H-TPP on Cu(111), because the azimuthal orientation and diffusion path of 2H-TPP at RT coincides with the crystallographic directions of Cu(111)[21]. The coverage of the Ni-TTBPBP monolayers on the Cu substrate was determined by STM and corresponded to 0.022 ML (1 ML defined as one molecule per atom of the substrate surface). Gas phase model structures of Ni-TTBPBP and its dehydrogenated congeners (cf. Figure 6) have been optimized using density-functional theory with the Turbomole program[35, 36] using the exchange-correlation functional due to Becke and Perdew in combination with the D3 van der Waals dispersion correction due to Grimme[37] and the def2-SV(P) basis set on all atoms. All optimized structures have been verified as true minima in the gas phase.

Results and discussion

To begin with, we briefly discuss the coverage-dependent adsorption behaviour of Ni-TTBPBP on Cu(111) at room temperature. A typical STM image of Ni-TTBPBP molecules at low coverage, which is 0.001 ML (5% of a full monolayer), is shown in Figure 2a: the previously featureless substrate steps are decorated with Ni-TTBPBP molecules, which can be discerned as single dots, with an intermolecular distance of ~1.6 nm, i.e. in the order of the size of the molecule. This observation evidences that at RT the molecules are mobile enough to diffuse to the step edges; such a step decoration is frequently reported for metal-tetraphenylporphyrin (M-TPP) on single-crystal metal surfaces[14, 21, 33].

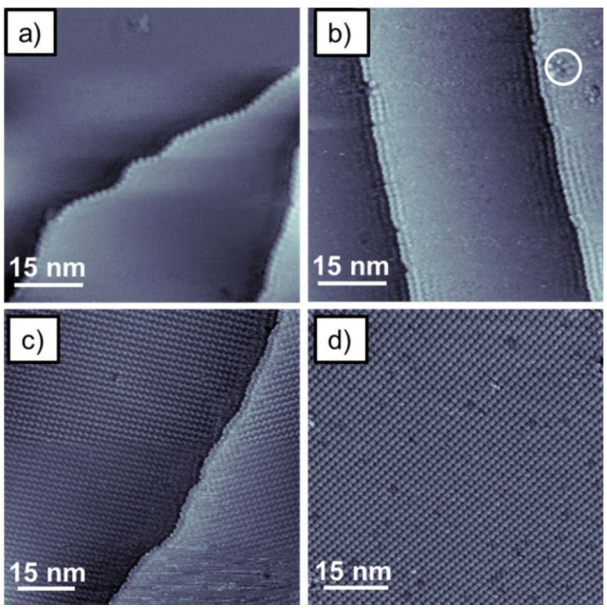

Figure 2. Constant current STM images of Ni-TTBPBP on Cu(111) as a function of the coverage: (a) 0.001 ML: step decoration (U = -1.28 V, I = 28.9 pA). (b) 0.007 ML: formation of small-area islands (U = +1.5 V, I = 28.5 pA). The white circle in b marks a substrate defect decorated with molecules. (c) 0.013 ML: formation of large-area islands (U = -1.37 V, I = 21.9 pA). (d) 0.022 ML: a full monolayer (U = -1.27 V, I = 26.9 pA).

Upon increasing the Ni-TTBPBP coverage to ~0.007 ML (32% of a full monolayer), in Figure 2b small two-dimensional (2D) islands are observed along the step edges, indicating that the molecules at the step edge act as nucleation points. Occasionally, small islands are also observed away from the step edges (indicated with a white circle), probably due to pinning at defect sites.

At ~0.013 ML (59% of a full monolayer), 2D long-range ordered islands with a square lattice self-assemble on the surface, as shown in Figure 2c. In addition to the islands, stripy features are observed, mainly along the scanning direction (see bottom of Figure 2c). They are attributed to fast diffusing molecules (much faster than the STM scanning speed) in a 2D gas phase of Ni-TTBPBP coexisting with the 2D islands[33, 38]. The existence of the 2D gas phase is confirmed by time sequences of STM images, which show attaching and detaching molecules at the island border.

When increasing the coverage to 0.022 ML (corresponding to a closed monolayer), the Cu(111) surface is completely covered by a well ordered Ni-TTBPBP layer with a square lattice; see Figure 2d. The Ni-TTBPBP molecules rarely adsorb on top of each other until the coverage exceeds one monolayer, confirming their high mobility at RT. The small number of depressions in the 2D islands under the given measurement condition probably originate from metal-free TTBPBP molecules, which are most likely already present in the Ni-TTBPBP material before evaporation onto the substrate[33, 39].

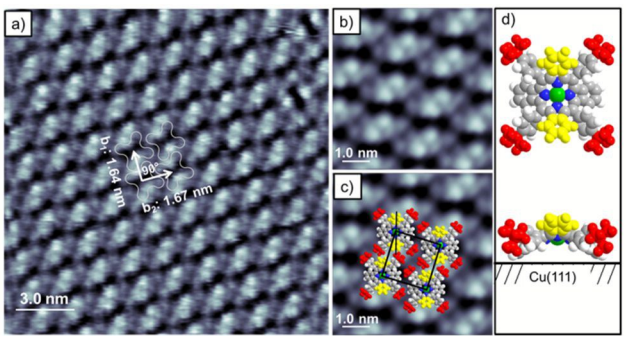

Figure 3. (a) Constant current STM image of the self-assembled 0.022 ML Ni-TTBPBP on Cu(111). The gray profiles indicate the position and orientation of individual molecules. A unit cell is also overlaid in the image. (b) Magnified and rotated detail of the central part of (a). (c) The micrograph from (b) superimposed with correspondingly scaled molecular models. The molecular axis (solid line) is rotated by 15° with respect to the unit cell. (d) Top view and side view of space-filling model of Ni-TTBPBP. In the model, the lifted benzene rings are displayed in yellow and the four tert-butyl groups in red. Tunnelling parameters: (a-c) U = -1.30 V, I = 28.4 pA.

As next step, we analyse the intramolecular conformation of Ni-TTBPBP on Cu(111). Figure 3a shows a high resolution STM image of one domain of the well-ordered Ni-TTBPBP molecules on Cu(111) at a coverage of ~0.022 ML. All molecules in a unit cell (domains) have an identical orientation, and the side length of the lattice vectors of the supramolecular assembly are b_1 = 1.64 ±0.02 nm and b_2 = 1.67±0.02 nm, with an angle of γ = 90°±1° between the two vectors, i.e. a square order within the margins of error. Figure 3b shows an enlarged section of the image depicted in Fig 3a. The molecules appear with a depression in the centre, along with two bright protrusions and four peripheral dim protrusions forming a square. The observed molecular appearance is found to be mainly independent of the polarity and value of the bias voltage in the range of -1.0 V to +1.4 V. Therefore, it is reasonable to assume that the appearance of Ni-TTBPBP on Cu(111) in STM is dominated by the topography of the molecule and not by its electronic structure[21, 40, 41].

To facilitate the identification of intramolecular features, the STM image in Figure 3c is superimposed with scaled models of Ni-TTBPBP. The intramolecular conformation of the molecular model was optimized in the gas phase, i.e. without accounting for interactions with the Cu substrate. Figure 3d shows the gas phase geometry with the following parameters: the twist angle of phenyl rings is roughly 45°, and the two pairs of opposite benzene rings are bent towards the surface or away from the surface by about 30°. Inspection of the optimized gas phase geometry (see the SI for details and atomic Cartesian coordinates) strongly suggests that the benzene rings highlighted yellow in Figure 3c will remain the most elevated part of the molecule even on the surface due to intramolecular steric repulsions with the adjacent phenyl rings. Based on this consideration along with the perfect fit of the superimposed models and the discussed domination of the topography contrast in STM, the two bright protrusions in the STM images are assigned to the upward bent benzene rings. In the following the symmetry axis through the upper benzene rings as indicated in Fig. 3c is referred to as the molecular axis. In addition, four dimmer protrusions are found in the ST micrograph at the position of the tert-butyl groups (marked red).

As mentioned above, the Ni-TTBPBP molecules form a well-ordered layer with a square unit cell with a lattice constant of ~1.6 nm. The molecular axes (through the upper benzene rings) exhibit an azimuthal angle of -15° or +15° with respect to the lattice vector b_1 of the unit cell. As a consequence, for each unit cell two different supramolecular arrangements are possible. These two different ordered structures can be transferred into each other only by a mirror operation (note that in this consideration the substrate is neglected). This property is referred to as organizational chirality, and was reported before for other porphyrin derivatives on metals surfaces[25, 33, 42, 43]. Overall, the adsorption behaviour of Ni-TTBPBP on Cu(111) thus can be regarded as another example of supramolecular chirality formed by non-chiral molecules and non-chiral surface. Identical azimuthal orientations of the individual molecules in respect to the supramolecular unit cell (-15° and +15°) have also been observed for tetraphenylporphyrins (TPPs) on coinage metal (111) surfaces[16, 21, 33]. Please note that while in some of the cited works the azimuthal angle is given as 30°, the actual orientations are identical since the molecular axis was defined differently in these cases. For TPPs, the supramolecular arrangement is governed by so-called T-type interactions between the phenyl rings of neighbouring porphyrins. Thereby the 4-position of one phenyl group points directly to the centre of a phenyl group of a neighbouring molecule. Since in Ni-TTBPBP one tert-butyl group is attached to the 4-position of each phenyl ligands, the T-type interaction cannot occur. From the molecular arrangement shown in Figure 3c, we instead propose that the attractive intermolecular interactions stabilizing the structure are caused by van der Waals forces between the tBP groups and possibly phenyl groups of neighbouring molecules[44].

After discussing the intramolecular conformation and intermolecular interaction of Ni-TTBPBP on Cu(111), we address the orientation of the unit cell and of the individual molecules in respect to the Cu substrate. In our STM images, we observe that the lattice vectors b_1 of the square unit cells are rotated by +15° or -15° with respect to the <110> high symmetry directions (close packed rows) of the substrate. Considering the substrate symmetry, this leads to 3 square unit cells, rotated to each other by 120° (or 30°); these three different unit cells are observed in STM images without

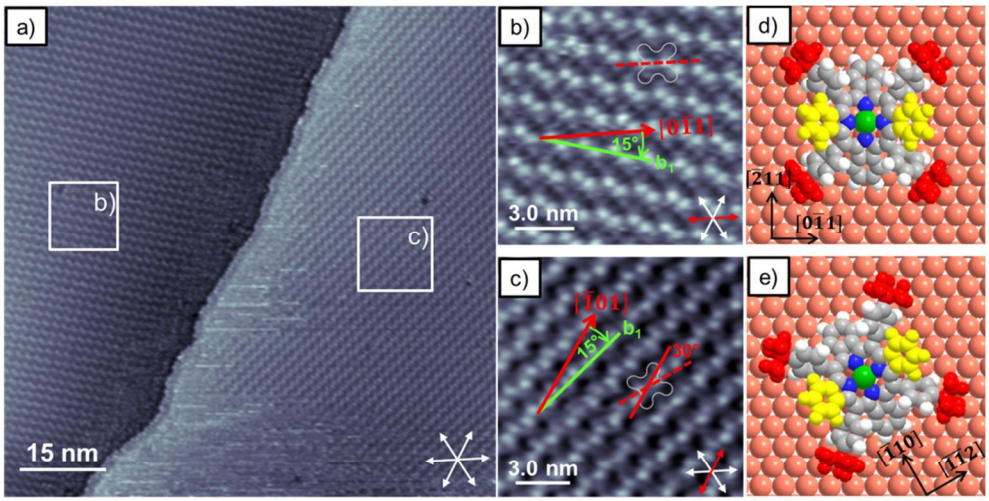

Figure 4. (a) Overview STM image of Ni-TTBPBP on Cu(111) at a coverage of 0.013 ML, displaying two domains. (b) and (c) zoom-ins of the regions indicated in (a). The grey profiles indicate the contour of an individual molecule. The dashed lines represent the molecular axis of the Ni-TTBPBP through the upward bent benzene rings. The solid line indicates one the three main substrate orientations. (d) and (e) Proposed models for the azimuthal orientation of molecules in (b) and (c), respectively. Image parameters: (a) U = -1.37 V, I = 21.9 pA; (b) U = -1.37 V, I = 22.0 pA; (c) U = -1.37 V, I = 21.9 pA.

submolecular resolution (not shown). Since the molecular axes (through the upper benzene rings) of the molecules in the unit cell are oriented +15° or -15° relative to the vector b_1 (see above), that is along the <110> and <211> substrate azimuths, the number of non-equivalent unit cells doubles to 6. If we, in addition, also allow that the molecular axis of molecule in the unit cell is rotated by 90° (that is +15° or -15° relative to the vector b_2), we altogether expect 12 different domains, 9 of which have actually been observed; for an overview of the 12 structures and the corresponding STM images see Figures S1 and S2 in the SI.

As illustrative example, a typical STM image of Ni-TTBPBP on Ni(111) at a coverage of ~0.013 ML is depicted in Fig 4a, with two domains separated by a step edge. Figure 4b and c depict zoom-ins of these two domains. The b_1 unit cell vectors (denoted as green arrows) are rotated by 60° with respect to each other, with both unit cells aligned +15° relative to the <110> directions of the Cu(111) surface (red arrows). Interestingly, the two domains have different chirality, that is, in (b) the molecular axes are rotated -15° (counter clockwise) to the b_1 vector while in (c) they are rotated +15° (clockwise). As a consequence, the molecular axes in (b) are aligned along the <110> direction, whereas in (c) they are rotated by 30°, that is, they are aligned along the <211> direction (see dashed red lines).

To discuss the specific orientations in more detail, tentative models are depicted in Figures 4d and 4e, reflecting the experimental findings in the neighbouring column. Since the adsorption site cannot be determined from our RT STM images, the metal centres of Ni-TTBPBP molecules were arbitrarily placed on hollow sites. In Figure 4d, the molecular axis through the upper benzene rings (indicated in yellow) is aligned along one of the <110> directions and in Figure 4e the other molecular axis (through the lower benzene rings) is aligned in this direction; in other words, the molecule is rotated by 90° (or 30°). Both orientations were found with equal probability when analysing numerous STM images (totally ~2 000 molecules were counted). In each geometry, one of the two connection lines of two opposite nitrogen atoms within the macrocycle coincides with the corresponding symmetry axes, indicating a clear energetic preference for this orientation. This could be due to an attractive interaction between the nitrogen atoms and the substrate Cu atoms; alternatively, one could also envisage that the specific registry of tert-butyl groups with the substrate contributes to the preference of the two specific orientations.

Next, we will focus on thermally induced conformational changes of Ni-TTBPBP on Cu(111). Figure 5a and 5b show the STM images acquired at RT after annealing ~0.022 ML Ni-TTBPBP at 400 K for 10 min. Interestingly, the supramolecular order with a square unit cell described above is not observed anymore, but instead domains with an oblique unit cell are found. Within these ordered domains, molecules with three different distinct appearances (motifs) can be clearly distinguished. These are marked by coloured squares in the insert of Figure 5b: motif 1 with two bright protrusions (black), motif 2 with one bright protrusion (yellow,) and motif 3 with four dim protrusions (red). Among them, motif 1 represents the intact molecule just as before annealing, while motif 2 and 3 are new species found after annealing. If we further heat the sample to 450 K, practically almost all molecules exhibit motif 3 (not shown here), which indicates that motif 2 is an intermediate state to motif 3 during annealing.

When applying the same annealing procedure (10 min @ 400 K) to a lower Ni-TTBPBP coverage of ~0.013 ML, similar changes are found; however, the number of modified appearances, that is motifs 2 and 3, is significantly larger than for the full monolayer. The corresponding STM images are depicted in Figure 5c and 5d (measured at 200 K because of the higher molecular mobility at lower coverage). Again, the coloured squares in Figure 5d highlight the three distinct motifs. For both coverages (0.013 ML and 0.022 ML), the supramolecular domains after annealing have practically the same order, and the corresponding lattice vectors are c_1 = 1.72 ±0.02 nm and c_2 = 1.73±0.02 nm, with an enclosed angle of γ = 104°±1° (indicated in Fig. 5d). Individual molecules within this long-range ordered oblique arrangement are orientated with their molecular axis along the close-packed <110> substrate orientation (c.f. Fig. 5d). Therefore, 6 different domains should

be formed if we further consider the molecular arrangement in the supramolecular structure, two of which can be observed on the upper part of Figure 5c. The different unit cells, square vs. oblique, for the supramolecular structures before and after annealing, respectively, indicate a change of the molecule-molecule and/or molecule-substrate interactions, which possibly originates from the change of intramolecular conformation[23, 45]. In addition, the area of the oblique unit cell (2.87±0.08 nm^2) slightly increases compared with that of square unit cell (2.74±0.07 nm^2).

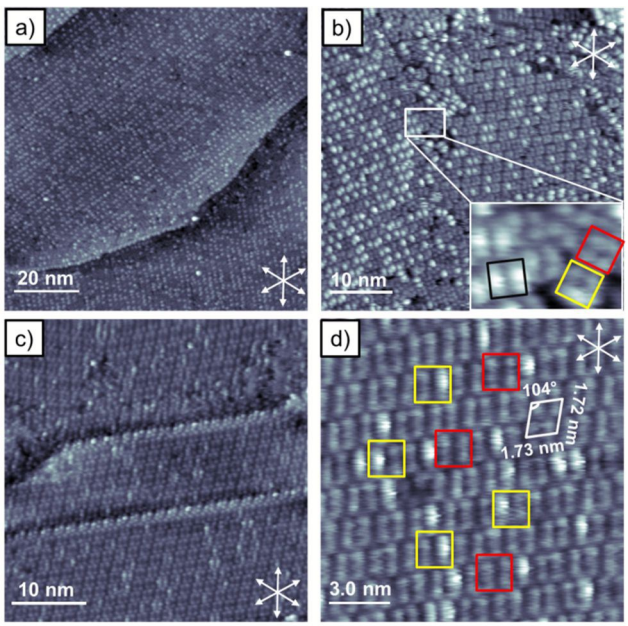

Figure 5. (a) and (b) STM images recorded after annealing ~0.022 ML Ni-TTBPBP on Cu(111) at 400 K for 10 min. (c) and (d) STM images after annealing ~0.013 ML Ni-TTBPBP on Cu(111) at 400 K for 10 min. A unit cell is overlaid in (d). Images (c) and (d) were imaged at 200 K because of the higher mobility compared to the 0.022 ML coverage. The colored squares in (b) and (d) highlight distinct appearances: motif 1 (black) with two-bright-protrusions, motif 2 (yellow) with one bright protrusion, and motif 3 (red) with four dim protrusions. Image parameters: (a) U = -1.18 V, I = 21.0 pA; (b) U = -1.18 V, I = 21.1 pA; (c) U = 0.99 V, I = 26.9 pA; (d) U = 0.99 V, I = 27.5 pA.

First, the nature of the thermally induced intramolecular modifications will be discussed before the coverage dependent yields will be addressed. The catalytic dehydrogenation of organic compounds by Cu is a well-known process in chemistry [46]. Recently, the dehydrogenation of porphyrin molecules on Cu surfaces has been reported. For example, Haq *et al.* proposed that on Cu(110) dehydrogenation of neighbouring porphyrins at elevated temperatures occurs[47]. Moreover, Vörden *et al.* demonstrated that the Cu(111) surface induced the transformation of octa-ethyl-porphyrin to tetra-benzo-porphyrin with an activation energy of ~1.2 eV[48]. Most relevant are the findings by Xiao *et al.*, who reported that the stepwise dehydrogenation of 2H-TPP on Cu(111) can be realized by annealing the sample at 400-500 K[23]; later on, Röckert *et al.* proved that this reaction depends on the surface coverage[45]. Based on the overall similarity of 2H-TPP and Ni-TTBPBP, and the very similar changes in the STM images, we suggest that the change of intramolecular conformation for Ni-TTBPBP on Cu(111) after annealing is mainly induced by the dehydrogenation of neighbouring carbon atoms (in the same molecule) along with the formation of new intramolecular C-C bonds.

Figure 6 depicts zoom-in ST micrographs of the three different motifs after annealing along with the proposed structural models. The geometries of the molecular models were optimized for the gas phase, without considering the interaction with the substrate (see experimental part). As discussed above, motif 1 corresponds to the intact Ni-TTBPBP molecule, with the two bright protrusions and four dim protrusions corresponding to the two upward benzene rings and four tert-butyl groups, respectively.

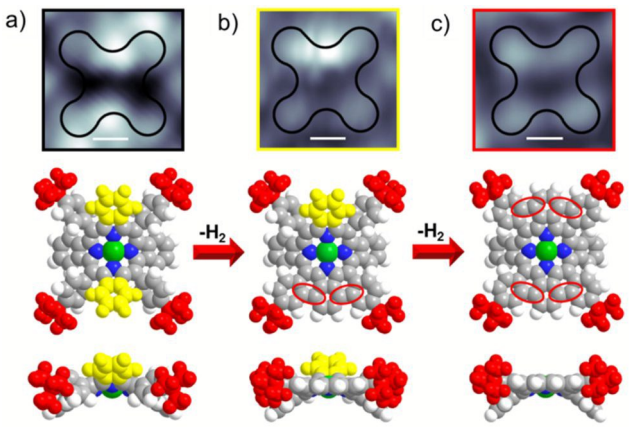

Figure 6. (a-c) High-resolution STM images of three different motifs and the proposed structural models for each motif. The black profiles indicate the structure of individual molecule before annealing. The red ellipses highlight the new formed C-C bonds in the respective model. The scale bar is 5.0 Å. Image parameters: (a) U = -1.30 V, I = 27.9 pA; (b) U = 1.22 V, I = 26.6 pA; (c) U = 1.22 V, I = -20.8 pA.

For motif 2, only one of the two dominant protrusions is visible anymore, while there is no apparent change to the four outer dimmer protrusions. Reconsidering that the ST micrographs mainly reflect the topography of the molecule one concludes that one half of the molecule is somewhat lowered after the annealing step. This can be realized by a lowering of one of the two upward benzene rings through partial dehydrogenation of the latter and the neighbouring phenyl groups, with a subsequent formation of C-C bonds between them; this is schematically shown in Figure 6b, where the red ellipses highlight the newly formed C-C bonds[23, 45]. Upon formation of such C-C bonds with both phenyl neighbours, the upward benzene ring and the involved phenyl rings fuse and "relax" to an orientation parallel to the surface. Consequently, the height of the fused benzene ring is lower than that of the tert-butyl groups, and therefore, the benzene ring cannot be observed in the STM image anymore. In contrast, the other upward benzene ring still exhibits a large tilt angle, and consequently, there is no conformation change and thus no change in the ST micrograph on this side. Aihara *et al.* reported on a similar structure achieved by thermal activation of the two alkynes of 2,3-dialkynylporphyrin in solution to undergo Bergman cyclization and subsequently form C-C bonds with two adjacent phenyl rings[49].

As for motif 3, a similar dehydrogenation step occurs successively at the remaining upward benzene ring; as a result,

	Annealing temperature T_a			
	400 K (θ=0.013 ML)	400 K (θ=0.022 ML)	450 K (θ=0.013 ML)	450 K (θ=0.022 ML)
Motif 1	0.5±0.4%	17.1±1.9%	0%	0%
Motif 2	12.3±3.2%	42.0±5.1%	1.7±0.9%	2.9±1.4%
Motif 3	87.2±3.7%	40.9±6.2%	98.3±0.9%	97.1±1.5%

Table 1. Occurance of the different motifs in percent (%), for different initial coverages, θ, after annealing for 10 min at different temperatures, T_a.

both benzene rings are lowered with respect to the surface and only four dim protrusions can be imaged (Figure 6c). One might anticipate that partial dehydrogenation might also occur on the downward benzene rings and consequently intramolecular C-C bonds can be formed between the fused phenyl rings and the downward benzene rings. However, in that case the molecule exhibits a pronounced bowl-like shape in the gas phase (see Figure S3 in the SI), which is not in agreement with our experimental observations. In particular, the asymmetric appearance of the molecule in Fig. 6c indicates that indeed the lower benzene rings remain "unfused". A similar square structure was also reported for 2H-TPP on Cu(111) after partial dehydrogenation[23, 45]. There, in the course of the dehydrogenation reaction of 2H-TPP, one phenyl group fuses with only one neighboring pyrrole ring in a specific fashion. We propose a similar dehydrogenative intramolecular aryl-aryl coupling reaction. Recently, similar thermally induced aryl-aryl coupling reactions have also been reported for gas-phase polycyclic aromatic hydrocarbons[50, 51]. Compared to these reports, the required temperature for the reaction in the present case is comparably low (only ~400K), which is attributed to the catalytic role of the Cu substrate[52, 53]. It is important to note that the annealing temperature of about 400 K, which is necessary to initiate the dehydrogenation reaction on Cu(111), is much lower than the temperature of the Knudsen cell used to thermally evaporate the molecules onto the surface (about 690 K), which again underlines the catalytic activity of the substrate.

Finally, we will discuss the influence of initial coverage on the annealing behaviour of Ni-TTBPBP on Cu(111). By comparing the annealing behaviour of Ni-TTBPBP at coverages of ~0.022 vs. ~0.013 ML (Figure 5a and 5c), we find that the yield for transformation to motifs 2 and 3 is higher for the lower coverage. Table 1 summarizes a statistical analysis of the different motifs (in total more than 4 000 Ni-TTBPBP molecules were counted) achieved at different annealing temperatures (400 and 450 K; both for 10 min) and initial coverages (0.022 and 0.013 ML). After annealing at 400 K, higher transformation yields are observed for the lower initial coverage, that is, 99.5% for 0.013 ML vs. 82.9% for 0.022 ML. Intriguingly, the percentage of motif 3 also decreases with increasing initial coverage from 87% for 0.013 ML to 41% for 0.022 ML. For comparison, after annealing at 450 K, the molecules practically completely transform to motif 3 for both coverages, with values 98% for 0.013 ML and 97% for 0.022 ML. Based on these observations, we state that the intramolecular dehydrogenation of Ni-TTBPBP on Cu(111) is coverage-dependent, with a lower yield at higher initial coverage.

Interestingly, a coverage-dependent dehydrogenation was also reported for Cu-TPP on Cu(111); the authors attributed this behaviour to a stabilizing effect of T-type interactions within the Cu-TPP islands formed at high coverage[45]. A similar explanation is also applicable to our experimental results. Because of the comparably weak molecule-substrate interaction, Ni-TTBPBP molecules are very mobile on Cu surface (note the required reduced STM acquisition temperature in Fig. 5 c and d) and they are present as a 2D gas that coexists with ordered islands below saturation of the monolayer[21, 23, 33]. The Ni-TTBPBP islands are stabilized by van der Waals interactions between neighbouring tert-butyl groups. Thus for the saturated monolayer dehydrogenation is less likely than in presence of a 2D gas phase. Furthermore, assuming that the dehydrogenation is catalysed by the Cu substrate, a reduced substrate C-H bond distance, which is certainly easier realized in the dynamic situation of the 2D-gas phase, promotes the reaction[45].

Conclusions

We have systematically investigated the adsorption behaviour and thermally induced transformation of Ni-TTBPBP on Cu(111) by means of STM. The characteristic supramolecular structure of Ni-TTBPBP is formed by the intermolecular van der Waals interactions, mediated by the tert-butyl groups of neighbouring molecules. Upon moderate heating, two irreversible intramolecular conformational changes are observed, which are caused by thermally induced intramolecular aryl-aryl dehydrogenation reaction. Moreover, this intramolecular structural change becomes slower at higher initial coverage, mainly because of the formation of large-area Ni-TTBPBP islands at that coverage. Our results are of great importance for a better understanding of the growth behaviour of benzoporphyrin family on metal surfaces and may shed light on tailoring the molecular properties via dehydrogenative intramolecular aryl-aryl coupling reaction.

Acknowledgements

The authors gratefully acknowledge the funding by the German Research Council (DFG) through research unit FOR 1878/funCOS, the Cluster of Excellence 'Engineering of Advanced Materials' (http://www.eam.uni-erlangen.de) and by the Collaborative Research Center SFB 953 at the Friedrich-Alexander-Universität Erlangen-Nürnberg. L.Z. thanks the Alexander von Humboldt Foundation for a research fellowship.

Notes and references

[a] Lehrstuhl für Physikalische Chemie II, Universität Erlangen-Nürnberg, Egerlandstr. 3, 91058 Erlangen, Germany.
Email: hubertus.marbach@fau.de
[b] Interdisciplinary Center for Molecular Materials (ICMM) Universität Erlangen-Nürnberg, Germany.
[c] Lehrstuhl für Organische Chemie II, Universität Erlangen-Nürnberg, Henkestr. 42, 91054 Erlangen, Germany..

[d] Lehrstuhl für Theoretische Chemie, Universität Erlangen-Nürnberg, Egerlandstr. 3, 91058 Erlangen, Germany.

† Electronic Supplementary Information (ESI) available: The atomic Cartesian coordinates for the calculated gas phase models and overview of the 12 structures as well as the corresponding STM images for Ni-TTBPBP on Cu(111). See DOI: 10.1039/b000000x/

1 J. V. Barth, G. Costantini and K. Kern, *Nature*, 2005, **437**, 671.
2. M. Chen, M. Röckert, J. Xiao, H.-J. Drescher, H.-P. Steinrück, O. Lytken and J. M. Gottfried, *J. Phys. Chem. C*, 2014, **118**, 8501.
3. S. Ditze, M. Stark, F. Buchner, A. Aichert, N. Jux, N. Luckas, A. Gorling, W. Hieringer, J. Hornegger, H.-P. Steinrück and H. Marbach, *J. Am. Chem. Soc.*, 2014, **136**, 1609.
4. S. Ditze, M. Stark, M. Drost, F. Buchner, H.-P. Steinrück and H. Marbach, *Angew. Chem. Int. Edit.*, 2012, **51**, 10898.
5. T. A. Jung, R. R. Schlittler and J. K. Gimzewski, *Nature*, 1997, **386**, 696.
6. H.-J. Gao and L. Gao, *Prog. Surf. Sci.*, 2010, **85**, 28.
7. F. Klappenberger, *Prog. Surf. Sci.*, 2014, **89**, 1.
8. M. Chen, X. F. Feng, L. Zhang, H. X. Ju, Q. Xu, J. F. Zhu, J. M. Gottfried, K. Ibrahim, H. J. Qian and J. O. Wang, *J. Phys. Chem. C*, 2010, **114**, 9908.
9. H. Marbach and H.-P. Steinrück, *Chem. Commun.*, 2014, **50**, 9034.
10. J. V. Barth, *Annu. Rev. Phys. Chem.*, 2007, **58**, 375.
11. J. K. Gimzewski and C. Joachim, *Science*, 1999, **283**, 1683.
12. M. Jurow, A. E. Schuckman, J. D. Batteas and C. M. Drain, *Coordin. Chem. Rev.*, 2010, **254**, 2297.
13. G. Di Santo, C. Sfiligoj, C. Castellarin-Cudia, A. Verdini, A. Cossaro, A. Morgante, L. Floreano and A. Goldoni, *Chem. Eur. J.*, 2012, **18**, 12619.
14. W. Auwärter, A. Weber-Bargioni, A. Riemann, A. Schiffrin, O. Groning, R. Fasel and J. V. Barth, *J. Chem. Phys.*, 2006, **124**, 194708.
15. Y. Bai, F. Buchner, I. Kellner, M. Schmid, F. Vollnhals, H.-P. Steinrück, H. Marbach and J. Michael Gottfried, *New J. Phys.*, 2009, **11**, 125004.
16. F. Buchner, K. Flechtner, Y. Bai, E. Zillner, I. Kellner, H.-P. Steinrück, H. Marbach and J. M. Gottfried, *J. Phys. Chem. C*, 2008, **112**, 15458.
17. F. Buchner, K. Seufert, W. Auwärter, D. Heim, J. V. Barth, K. Flechtner, J. M. Gottfried, H.-P. Steinrück and H. Marbach, *ACS Nano*, 2009, **3**, 1789.
18. K. Diller, F. Klappenberger, M. Marschall, K. Hermann, A. Nefedov, C. Woll and J. V. Barth, *J. Chem. Phys.*, 2012, **136**, 014705.
19. S. Ditze, M. Röckert, F. Buchner, E. Zillner, M. Stark, H.-P. Steinrück and H. Marbach, *Nanotechnology*, 2013, **24**, 115305.
20. J. M. Gottfried, K. Flechtner, A. Kretschmann, T. Lukasczyk and H.-P. Steinrück, *J. Am. Chem. Soc.*, 2006, **128**, 5644.
21. F. Buchner, E. Zillner, M. Rockert, S. Glassel, H.-P. Steinrück and H. Marbach, *Chem. Eur. J.*, 2011, **17**, 10226.
22. M. Stark, S. Ditze, M. Drost, F. Buchner, H.-P. Steinrück and H. Marbach, *Langmuir*, 2013, **29**, 4104.
23. J. Xiao, S. Ditze, M. Chen, F. Buchner, M. Stark, M. Drost, H.-P. Steinrück, J. M. Gottfried and H. Marbach, *J. Phys. Chem. C*, 2012, **116**, 12275.
24. M. In't Veld, P. Iavicoli, S. Haq, D. B. Amabilino and R. Raval, *Chem. Commun.*, 2008, **13**, 1536.
25. D. E. Barlow and K. Hipps, *J. Phys. Chem. C*, 2000, **104**, 5993.
26. G. Di Santo, S. Blankenburg, C. Castellarin-Cudia, M. Fanetti, P. Borghetti, L. Sangaletti, L. Floreano, A. Verdini, E. Magnano, F. Bondino, C. A. Pignedoli, M.-T. Nguyen, R. Gaspari, D. Passerone and A. Goldoni, *Chem. Eur. J.*, 2011, **17**, 14354.
27. G. Di Santo, C. Sfiligoj, C. Castellarin-Cudia, A. Verdini, A. Cossaro, A. Morgante, L. Floreano and A. Goldoni, *Chem. Eur. J.*, 2012, **18**, 12619.
28. J. Brede, M. Linares, S. Kuck, J. Schwobel, A. Scarfato, S. H. Chang, G. Hoffmann, R. Wiesendanger, R. Lensen, P. H. J. Kouwer, J. Hoogboom, A. E. Rowan, M. Broring, M. Funk, S. Stafstrom, F. Zerbetto and R. Lazzaroni, *Nanotechnology*, 2009, **20**, 275602.
29. F. Klappenberger, A. Weber-Bargioni, W. Auwärter, M. Marschall, A. Schiffrin and J. V. Barth, *J. Chem. Phys.*, 2008, **129**, 214702.
30. F. Buchner, K. Comanici, N. Jux, H.-P. Steinrück and H. Marbach, *J. Phys. Chem. C*, 2007, **111**, 13531.
31. L. Grill, M. Dyer, L. Lafferentz, M. Persson, M. V. Peters and S. Hecht, *Nature Nanotech.*, 2007, **2**, 687.
32. F. Buchner, J. Xiao, E. Zillner, M. Chen, M. Röckert, S. Ditze, M. Stark, H.-P. Steinrück, J. M. Gottfried and H. Marbach, *J. Phys. Chem. C*, 2011, **115**, 24172.
33. F. Buchner, I. Kellner, W. Hieringer, A. Görling, H.-P. Steinrück and H. Marbach, *Phys. Chem. Chem. Phys.*, 2010, **12**, 13082.
34. I. Horcas, R. Fernandez, J. M. Gomez-Rodriguez, J. Colchero, J. Gomez-Herrero and A. M. Baro, *Rev. Sci. Instrum.*, 2007, **78**, 013705.
35. R. Ahlrichs, F. Furche, C. Hättig, W. M. Klopper, M. Sierka and F. Weigend, *TURBOMOLE 6.6*, University of Karlsruhe, since 1988; www.turbomole.com.
36. R. Ahlrichs, M. Bär, M. Häser, H. Horn and C. Kölmel, *Chem. Phys. Lett.*, 1989, **162**, 165.
37. S. Grimme, J. Antony, S. Ehrlich and H. Krieg, *J. Chem. Phys.*, 2010, **132**, 151104.
38. D. E. Barlow, L. Scudiero and K. Hipps, *Langmuir*, 2004, **20**, 4413.
39. K. Comanici, F. Buchner, K. Flechtner, T. Lukasczyk, J. M. Gottfried, H.-P. Steinrück and H. Marbach, *Langmuir*, 2008, **24**, 1897.
40. S.-H. Chang, S. Kuck, J. Brede, L. Lichtenstein, G. Hoffmann and R. Wiesendanger, *Phys. Rev. B*, 2008, **78**, 233409.
41. F. Buchner, K. G. Warnick, T. Wolfle, A. Görling, H.-P. Steinrück, W. Hieringer and H. Marbach, *J. Phys. Chem. C*, 2009, **113**, 16450.
42. Z. Cheng, L. Gao, Z. Deng, Q. Liu, N. Jiang, X. Lin, X. He, S. Du and H.-J. Gao, *J. Phys. Chem. C*, 2007, **111**, 2656.
43. S. M. Barlow and R. Raval, Surf. Sci. Rep., 2003, **50**, 201.
44. M. Xi, M. X. Yang, S. K. Jo, B. E. Bent and P. Stevens, *J. Chem. Phys.*, 1994, **101**, 9122.
45. M. Röckert, M. Franke, Q. Tariq, S. Ditze, M. Stark, P. Uffinger, D. Wechsler, U. Singh, J. Xiao, H. Marbach, H.-P. Steinrück and O. Lytken, *Chem. Eur. J.*, 2014, **20**, 8948.
46. T. Punniyamurthy and L. Rout, *Coordin. Chem. Rev.*, 2008, **252**, 134.
47. S. Haq, F. Hanke, M. S. Dyer, M. Persson, P. Iavicoli, D. B. Amabilino and R. Raval, *J. Am. Chem. Soc.*, 2011, **133**, 12031.
48. D. van Vorden, M. Lange, M. Schmuck, J. Schaffert, M. C. Cottin, C. A. Bobisch and R. Moller, *J. Chem. Phys.*, 2013, **138**, 211102.
49. H. Aihara, L. Jaquinod, D. J. Nurco and M. Smith, *Angew. Chem. Int. Edit.*, 2001, **40**, 3439.

50. A. W. Amick and S. E. Martin, *Aust. J. Chem.*, 2014, **67**, 1338.
51. X. Xue and L. T. Scott, *Org. Lett.*, 2007, **9**, 3937.
52. M. Treier, C. A. Pignedoli, T. Laino, R. Rieger, K. Müllen, D. Passerone and R. Fasel, *Nature Chem.*, 2011, **3**, 61.
53. Q. Sun, C. Zhang, H. Kong, Q. Tan and W. Xu, *Chem. Commun.*, 2014, **50**, 11825.

